Article

High-Entropy Diborides – Silicon Carbide Composites by Reactive and Non-reactive Spark Plasma Sintering: A Comparative Study

Ekaterina Pakhomova , Giacomo Cao , Roberto Orrù * , Roberta Licheri , Paolo Ferro , And Roberta Licheri

Posted Date: 22 December 2023

doi: 10.20944/preprints202312.1708.v1

Keywords: high-entropy borides; silicon carbide; spark plasma sintering; self-propagating high-temperature synthesis; resistance to oxidation; fracture toughness

Article

High-Entropy Diborides—Silicon Carbide Composites by Reactive and Non-Reactive Spark Plasma Sintering: A Comparative Study

Ekaterina Pakhomova [1], Giacomo Cao [1], Roberto Orrù [1,*], Sebastiano Garroni [2], Paolo Ferro [3] and Roberta Licheri [1]

[1] Dipartimento di Ingegneria Meccanica, Chimica, e dei Materiali, Unità di Ricerca del Consorzio Interuniversitario Nazionale per la Scienza e Tecnologia dei Materiali (INSTM), Università degli Studi di Cagliari, via Marengo 2, 09123 Cagliari, Italy; ekaterina.pakhomova@unica.it, giacomo.cao@unica.it, roberta.licheri@unica.it

[2] Dipartimento di Scienze Chimiche, Fisiche, Matematiche e Naturali, Università degli Studi di Sassari, 07100, Sassari, Italy; sgarroni@uniss.it

[3] Dipartimento di Tecnica e Gestione dei Sistemi Industriali, Università di Padova, Stradella S. Nicola 3, 36100 Vicenza, Italy; paolo.ferro@unipd.it

* Correspondence: roberto.orru@unica.it; Tel.: (+39-070-6755076)

Abstract: The Reactive Spark Plasma Sintering (R-SPS) method is compared in this work with the two-steps SHS-SPS route, based on combination of the Self-propagating High-temperature Synthesis (SHS) with the SPS process, for the fabrication of dense $(Hf_{0.2}Mo_{0.2}Ti_{0.2}Ta_{0.2}Nb_{0.2})B_2$-SiC and $(Hf_{0.2}Mo_{0.2}Ti_{0.2}Ta_{0.2}Zr_{0.2})B_2$-SiC ceramics. A multiphasic and inhomogeneous product, containing various borides, is obtained at 2000°C/20min by R-SPS, from transition metals, B_4C and Si. In contrast, if the same precursors are first reacted by SHS, and then processed by SPS under the optimized condition of 1800°C/20min, the desired ceramics are successfully attained. Both High-Entropy-Boride/SiC products display densities > 97%, uniform microstructures and contained only small amounts of residual oxides (<2.4 wt.%). The presence of SiC makes the sintering temperature milder, i.e. 150°C below to that needed by the corresponding additive-free system. Fracture toughness is also markedly improved, particularly when considering the Nb-containing system processed at 1800°C/20min, whereas K_{IC} progressively decreases (from 7.35 to 5.36 MPa $m^{1/2}$) as the SPS conditions become more severe. SiC addition is found to inhibit the volatilization of metal oxides like MoO_3 formed during oxidation experiments, thus avoiding mass loss in the ceramics. The benefits above also likely take advantage of the fact that the two composite constituents are synthesized in parallel, according to the SHS-SPS approach, rather than being produced separately and combined subsequently, so that strong interfaces between them are formed.

Keywords: high-entropy borides; silicon carbide; spark plasma sintering; self-propagating high-temperature synthesis; resistance to oxidation; fracture toughness

1. Introduction

The need of structural components able to operate under harsh conditions (high-temperatures, elevated heat fluxes, oxidation, and corrosive environments, neutrons irradiations, etc.) encountered in various application fields (aerospace, metallurgy, nuclear, etc.) prompts for the development of Ultra High Temperature Ceramics (UHTCs) able to face such requirements [1]. To this aim, a significant effort was made to identify suitable processing techniques for their obtainment in bulk form and the related characterization. The attention was mostly focused on individual transition metal borides (ZrB_2, HfB_2, TaB_2, etc.) and carbides (ZrC, HfC, TaC, etc.) [2,3]. The introduction of proper amounts of Si-containing additives (SiC, $MoSi_2$, $HfSi_2$, etc.) to latter systems was found to

 doi:10.20944/preprints202312.1708.v1

facilitate the consolidation of their difficult-to-sinter powders as well as concurrently improve oxidation resistance and mechanical properties [4–6].

In the last decade, a great attention was given to High-Entropy Borides (HEBs), a recently discovered sub-class of UHTCs resulting from the combination, in near-equimolar ratio, of 4-5 individual metal borides, to generate single-phase crystalline solid solutions with maximum configurational entropy and, consequently, superior thermodynamic stability at high temperatures [7]. Members of HEBs were reported to shown better properties, as compared to their single boride constituents [7–9]. The experimental and computational results obtained so far have been critically examined in two recent review papers, in view of the possible exploitation of such systems for applications under extreme environments [10,11]. The need of additional studies from both the experimental and theoretical viewpoints has been emphasized to enhance the understanding of such novel and complex UHTCs.

As for the case of individual borides, additive-free HEBs unavoidably suffer of insufficient oxidation resistance at high temperatures as well as low fracture toughness. Therefore, the presence of the secondary Si-containing phases mentioned above is expected to improve the latter properties also in multi-metallic diborides systems, other than making their powders consolidation easier. Accordingly, few studies have been recently addressed to the combination of some HEBs with SiC [12–16]. For instance, the mixture obtained after adding α-SiC to HEB powders synthesized by borocarbothermal reduction (BCR, 1600°C/1h/10°Cmin^{-1}/vacuum) of metal oxides with B_4C was processed by SPS to produce $(Hf_{0.2}Zr_{0.2}Nb_{0.2}Ta_{0.2}Ti_{0.2})B_2$-20vol.%SiC [12,13]. It was found that the presence of the additive promoted sample densification, led to a refined product microstructure and improved fracture toughness through crack deflection and branching mechanisms. Following a similar approach, dense $(Hf_{0.2}Zr_{0.2}Mo_{0.2}Nb_{0.2}Ti_{0.2})B_2$-20vol.%SiC and $(Hf_{0.2}Mo_{0.2}Ta_{0.2}Nb_{0.2}Ti_{0.2})B_2$-20vol.%SiC were prepared at 2000°C by SPS starting from powders synthesized either by BCR or borothermal reduction (BR) [14]. It was reported that bulk ceramics from BCR powders displayed fine-grained microstructure and superior Vickers' hardness, whereas higher fracture toughness corresponded to samples obtained from BR powders. The BCR route was also used to synthesize (V,Ti,Ta,Nb)B_2-20.8 wt%SiC powders and the electromagnetic absorption properties of the obtained product was investigated [15]. Finally, $(Hf_{0.2}Zr_{0.2}Nb_{0.2}Ta_{0.2}Ti_{0.2})$-x SiC (x=0, 10, 20, 30%vol.) were also fabricated by the BCR-SPS approach [16]. In the latter study, the introduction of SiC particles was confirmed to improve powder consolidation and inhibit HEB grain growth during SPS (1800°C/10min/30MPa). Moreover, an increase of SiC content was found to enhance Vickers hardness (from ~19.5 to ~21GPa) and K_{IC} values, because of the synergic effect produced by grain refinement, and the presence of the carbide phase.

So far, no attention was given to the oxidation properties of HEB-SiC systems. In addition, only the few ceramic compositions mentioned above have been investigated.

In this work, the synthesis and simultaneous consolidation of $(Hf_{0.2}Mo_{0.2}Ti_{0.2}Ta_{0.2}Nb_{0.2})B_2$-SiC is first attempted by reactive SPS (R-SPS) starting from elemental transition metals, Si and B_4C. Alternatively, the two-steps SHS-SPS route, successfully employed for the obtainment of various quinary HEBs [9,17–18] is employed. In the latter, the same precursors used during R-SPS are reacted by Self-propagating High-temperature Synthesis (SHS), and the resulting powders are subsequently processed by SPS at different temperatures and processing times. In particular, the SHS-SPS method is adopted for the obtainment of $(Hf_{0.2}Mo_{0.2}Ti_{0.2}Ta_{0.2}Nb_{0.2})B_2$-SiC and $(Hf_{0.2}Mo_{0.2}Ti_{0.2}Ta_{0.2}Zr_{0.2})B_2$-SiC systems. The densification behavior of SHS powders is analyzed and compared with that displayed by the corresponding additive-free counterparts. Mechanical properties and oxidation behavior at high temperatures of the sintered ceramics are finally evaluated and compared.

2. Materials and Methods

Table 1 reports the characteristics of starting powders used in this work for the preparation of $(Hf_{0.2}Mo_{0.2}Ti_{0.2}Ta_{0.2}Me_{0.2})B_2$-SiC (with Me= Nb or Zr) by R-SPS and SHS, according to the following reaction stoichiometry:

$$0.4Hf + 0.4Mo + 0.4Ti + 0.4Ta + 0.4Me + Si + B_4C \rightarrow 2(Hf_{0.2}Mo_{0.2}Ti_{0.2}Ta_{0.2}Me_{0.2})B_2 + SiC \quad (1)$$

 doi:10.20944/preprints202312.1708.v1

which correspond approximately to $(Hf_{0.2}Mo_{0.2}Ti_{0.2}Ta_{0.2}Nb_{0.2})B_2$-27.7 vol.%SiC and $(Hf_{0.2}Mo_{0.2}Ti_{0.2}Ta_{0.2}Zr_{0.2})B_2$-27.4 vol.%SiC, respectively. For the sake of brevity, the two composite systems will be hereafter indicated as HEB_Nb-SiC and HEB_Zr-SiC respectively.

Table 1. Characteristics of precursors used for the synthesis of HEB_Nb-SiC and HEB_Zr-SiC by R-SPS and SHS.

Reactant	Vendor (code)	Particle size (μm)	Purity (%)
Hf	Alfa Aesar (10201	< 44	99.6
Mo	Alfa Aesar (10031)	< 149	≥ 99
Ta	Alfa Aesar (00337)	< 44 μm	99.8
Ti	Aldrich (26.849-6)	< 149 μm	99.7
Nb	Alfa Aesar (010275)	< 44	99.8
Zr	Thermo Scientific (00847)	2-3 μm	-
Si	Aldrich (21561-9)	< 44 μm	99%
B4C	Alfa Aesar (40504)	1-7 μm	99.4

About 20 g of powder were mixed for 20 min in a plastic vial equipped with 10 zirconia balls using a Horizontal Roller Ball Mill (mod. BML-2, Witeg Labortechnik GmbH, Germany). The resulting mixtures were processed either by reactive SPS or SHS. In the latter case, about 7 g of the mixture were cold pressed to form cylindrical pellets (10 mm diameter, 20-22 mm height) to be reacted by SHS inside a stainless-steel chamber first evacuated and then filled with Argon. An electrically heated tungsten filament was used to activate the synthesis reaction. Further details of SHS experiments can be found elsewhere [19]. The reacted products received a 20 min ball milling treatment in a SPEX 8000 (SPEX CertiPrep, USA) shaker mill, with stainless steel vial and steel balls (ball to powder weight ratio equal to 2). Laser light scattering analysis (CILAS 1180, France) was employed to determine particle size of the resulting powders.

The consolidation process was performed using an SPS apparatus (515S model, Fuji Electronic Industrial Co., Ltd., Kanagawa, Japan) under vacuum conditions (about 20 Pa). Approximately 3.5 (HEB_Zr-SiC) or 3.7 g (HEB_Nb-SiC) of powders were placed inside a cylindrical graphite die (30 mm external diameter; 15 mm inside diameter; 30 mm height) equipped with two punches (14.7 mm diameter, 20 mm height). SPS runs were conducted under temperature-controlled mode using an infrared pyrometer (CHINO, mod. IR-AHS2, Japan) focused on the lateral surface of the die. Temperature was increased at a constant rate (HR=200°C/min) from the room value to the maximum level (T_D). The sample was then maintained at T_D for a prescribed duration, in the range 5-20 min. The effect of T_D on the density, and composition of the SPS product was investigated in the range 1500–1900 °C. A mechanical pressure of 20 MPa was applied during the entire experiment duration. For the sake of reproducibility, each experiment was repeated at least twice.

The same sintering equipment, ancillary devices and die/plungers mentioned above are also used for directly processing the initial precursors listed in Table 1 by reactive SPS according to reaction (1). A relatively higher holding temperature (T_D=2000°C) was adopted in the latter case, compared to that considered with the SHS-SPS approach, while the heating rate was lowered (HR=100°C/min instead of 200°C/min). The dwell time at T_D and the applied pressure were set to 20 min, and 20 MPa, respectively.

Before being further characterized, bulk products obtained by SHS-SPS or R-SPS were cut, ground, and polished using progressively finer abrasive paper. The Archimedes' method was used to evaluate their absolute densities using distilled water as immersing medium. The corresponding relative densities were calculated by considering the theoretical values of 7.15 g/cm^3 (HEB_Nb-SiC) and 7.06 g/cm^3 (HEB_Zb-SiC) for the composite systems. The latter ones were evaluated by applying a rule of mixture [20] and using 8.67 g/cm^3 (HEB_Nb) [18], 8.52 g/cm^3 (HEB_Zr) [18] and 3.21 g/cm^3 (SiC) [21] as theoretical densities for the individual ceramic constituents.

Phases identification and structural characteristics of the SHS powders, R-SPS and SHS-SPS samples were determined by X-ray diffraction analysis (rotating anode SmartLab Rigaku, Japan and

 doi:10.20944/preprints202312.1708.v1

Philips PW 1830, Netherlands) using Cu K_α radiation, over a range of scattering angles 2ϑ from 10 to 130, in steps of 0.05° with 15 s acquisition time per angle. Phases amount and microstructural parameters were estimated with the Rietveld method by analyzing the XRD patterns with the MAUD program [22].

High resolution scanning electron microscopy (HRSEM) (mod. S4000, Hitachi, Tokyo, Japan) equipped with a UltraDry EDS Detector (Thermo Fisher Scientific, Waltham, MA, USA) was used to examine the microstructure as well as compositional homogeneity in the sintered samples.

Oxidation tests on sintered samples were performed in air using a muffle furnace (LT 24/11/B410, Nabertherm, Lilienthal, Germany). During these experiments, samples were heated at a rate of 5 °C/min from room temperature to a maximum value, in the range of 600-1300°C, followed by an isothermal step of 1h duration. Composition and the microstructure of the treated specimens was then examined by XRD and SEM.

Mechanical properties were determined by means of Micro Vickers Hardness Testers FUTURE-TECH FM-810 (Kawasaki, Kanagawa 210-0804, Japan). Samples were embedded into phenolic resin and then lapped and polished. A load of 1 N was applied with a loading time of 15 seconds. At least 5 measurements were performed for each sample, and the average values were then calculated. The fracture toughness was evaluated, using a load of 1 N in order to make cracks propagate from the indent tips. The scanning electron microscope (SEM)) Quanta 400 of Field Electron and Ion Company (Hillsboro, Oregon, United States) was used to determinate the crack length.

Fracture toughness was then calculated based on the crack lengths, according to Evans and Charles equation [23,24], namely:

$$K_{IC} = 0.0824 \frac{P}{c^{3/2}} \quad (2)$$

where K_{IC} is the fracture toughness, P the load, c the average crack length measured from the indentation center.

3. Results and discussion

3.1. Reactive Spark Plasma Sintering route

The simultaneous synthesis and consolidation of HEB_Nb-SiC by R-SPS was first attempted. This approach was successfully adopted in the literature for the preparation of dense ZrB_2-SiC from Zr, B_4C and Si [**25**]. When the starting reactants were processed for 20 min by SPS at T_D = 1900°C, with a heating rate of about 200°C/min, a nearly full dense ceramic composite (relative density >99.5%) was correspondingly obtained. To the same aim, in the present work the powder mixture consisting of initial precursors according to reaction (1) with Me=Nb were processed for 20 min by SPS at 2000°C with a non-isothermal heating time (t_H) of 20 min (heating rate of 100°C/min). The more severe sintering temperature (2000°C) considered here compared to that (1900°C) used for the preparation of ZrB_2-SiC was to facilitate the diffusion of the different metals contained in the HEB matrix across the material volume. The relatively lower heating rate applied in the present work also contribute to achieve the same purpose. In addition, such condition was also aimed to avoid the occurrence of the exothermic synthesis reaction (1) under the combustion mode. Indeed, as demonstrated in previous works [26,27], the latter regime, which is undesirable due to a series of negative drawbacks (residual porosity, not homogeneous products, die/plungers breakage, safety problems, etc.), is more likely established when operating at relatively higher heating rates. The sample shrinkage time profile recorded during R-SPS experiment is plotted in Figure 1 along with the imposed temperature pattern. It is seen that powder consolidation takes place in a gradual manner, mostly during the non-isothermal heating step. When the T_D value is reached, sample shrinkage further increases but a much slower rate. Based on the sintering curve shown in Figure 1, the occurrence of combustion-like reactions can be readily excluded, since a sudden change of the latter parameter is manifested when such an event takes place during R-SPS. This is what happened also during the preparation of ZrB_2-SiC by R-SPS, with the initial reactants gradually transformed to the final composite until the complete conversion was attained [25].

Preprints (www.preprints.org) | NOT PEER-REVIEWED | Posted: 22 December 2023 doi:10.20944/preprints202312.1708.v1

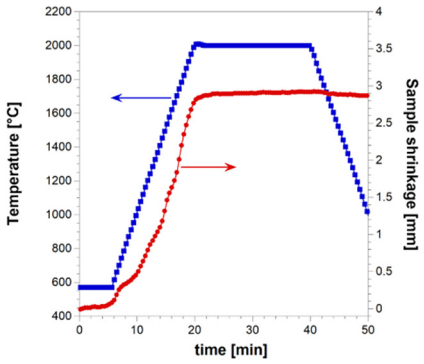

Figure 1. Temporal profiles of temperature and sample shrinkage recorded during the preparation of dense HEB_Nb-SiC by reactive SPS (T_D=2000 °C, HR=100°C/min, t_D=20 min, P=20 MPa).

The absolute density of the HEB_Nb-SiC based ceramic produced in this work was 6.88 ±0.12 g/cm^3, corresponding to a relative density of 96.2±1.6%.

The X-ray diffraction pattern, experimental and the best fit, of the R-SPSed product is reported in Figure 2. The corresponding structural and microstructural parameters estimated by the Rietveld analysis are summarized in Supplementary Table S1. The resulting sample is characterized by a mixture of phases which consist, according to the Rietveld analysis performed (R_{wp} = 9.6 %), of two solid solutions of $(Hf_{0.2}Ta_{0.2}Nb_{0.2}Mo_{0.2}Ti_{0.2})B_2$, with slightly different cell parameters, SiC, but also other binary and individual diborides, namely $(Ta_{0.5}Ti_{0.5})B_2$, MoB_2, and NbB_2. The total amount of undesired secondary phases resulted to be above 40 wt.% (Table S1), so that the obtainment by reactive SPS of the desired HEB-SiC product is far from being achieved.

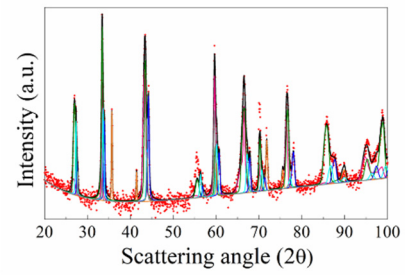

Figure 2. XRD pattern and related Rietveld refinement of HEB_Nb-SiC product obtained by Reactive SPS (T_D=2000 °C, HR=100°C/min, t_D=20 min, P=20 MPa) according to reaction (1) with Me=Nb.

SEM/EDS observations (cf. Figure 3) are consistent with XRD outcomes. The SEM micrograph confirms the high densification level reached during the process. However, the same micrograph and the corresponding elemental EDS maps also evidenced that the sintered sample display a very inhomogeneous microstructure. It is then possible to conclude that, as for the additive free HEB_Nb system investigated by Tallarita et al. [9], and despite the relatively higher temperature (2000°C) adopted in this work, the R-SPS approach did not provide the required conditions for synthesizing the corresponding HEB-SiC ceramic.

Preprints (www.preprints.org) | NOT PEER-REVIEWED | Posted: 22 December 2023 doi:10.20944/preprints202312.1708.v1

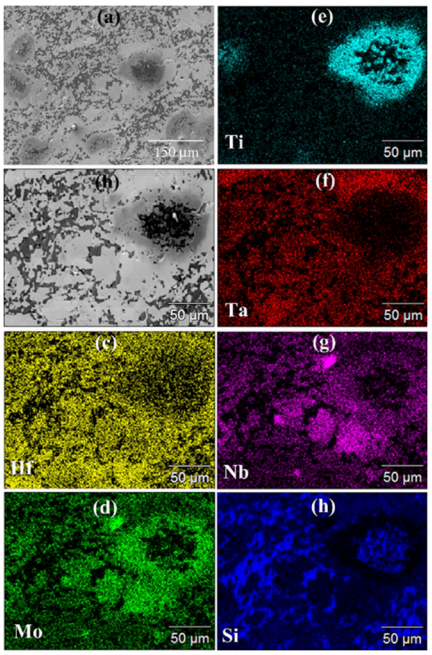

Figure 3. General (a) and detailed (b) SEM views along with the corresponding Hf (c), Mo (d), Ti (e), Ta (f), Nb (g), and Si (h) EDS maps of the HEB_Nb-SiC sample obtained by R-SPS (T_D =2000°C, HR=100°C/min, t_D=20min, P=20MPa) according to reaction (1) with Me=Nb.

3.2. SHS-SPS route

3.2.1. The $(Hf_{0.2}Mo_{0.2}Ti_{0.2}Ta_{0.2}Nb_{0.2})B_2$-SiC system

As described in section 3.1, the attempt to make the direct synthesis and consolidation of HEB_Nb-SiC by R-SPS failed. To achieve such goal, these two steps were then conducted separately, using the SHS-SPS approach. During the first processing stage, precursors, combined according to reaction (1) with Me=Nb, were first reacted by SHS. As for the synthesis of additive free $(Hf_{0.2}Mo_{0.2}Ti_{0.2}Ta_{0.2}Nb_{0.2})B_2$ from elemental reactants [9], also the exothermic reaction (1) displayed a self-sustaining character. The observed behavior was like that seen with the preparation of ZrB_2-SiC [25] and HfB_2-SiC [28] from Zr or Hf, B_4C, and Si, respectively. On the other hand, a preliminarily mechanical treatment was required to induce the SHS reaction in the TaB_2-SiC system [10]. The latter studies also evidenced that, when a single transition metal is involved, such a synthesis technique was able to lead to the desired MeB_2-SiC product with no secondary phases.

The transformation of the initial reactants to the desired HEB_Nb and SiC phases was verified by examining the SHS product by XRD and SEM.

XRD results are shown in Figure 4a, while the related structural and microstructural parameters are reported in supplementary Table S2. As emerged by the Rietveld refinement, SHS powders present a multiphasic product, made of the desired $(Hf_{0.2}Ta_{0.2}Nb_{0.2}Mo_{0.2}Ti_{0.2})B_2$ solid solution (14.9 wt.%), and SiC (11.5 wt.%) phases, with various additional metal borides, namely, HfB_2 (9.0 wt.%), TaB_2 (14.6 wt.%), NbB_2 (12.8 wt.%), TiB_2 (13.4 wt.%), MoB_2 (9.5 wt.%), and $(MoTiB_4)_2$ (3.9%). Furthermore, lower amounts (less than 3.0 wt.%) of $MoSi_2$, C, Si, SiO_2, B_4C have been also detected.

Preprints (www.preprints.org) | NOT PEER-REVIEWED | Posted: 22 December 2023 doi:10.20944/preprints202312.1708.v1

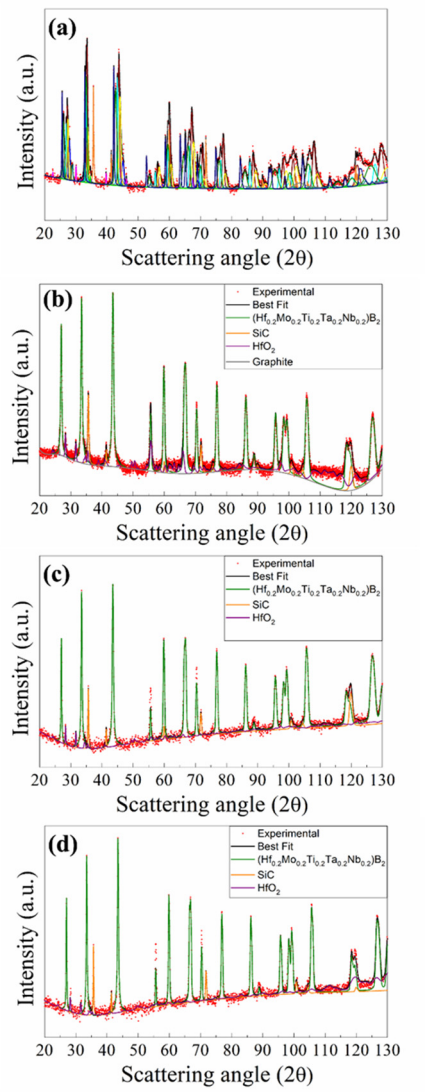

Figure 4. XRD pattern and related Rietveld refinement of SHS (a) and corresponding bulk samples obtained at different SPS conditions (20 MPa, HR=200°C/min): (b) 1800°C/20min, (c) 1900°C/5min, and (d) 1900°C/20min.

Table 2 reports particles size analysis results of the powders after ball milling the SHSed samples. Fine particles, with average size slightly larger than 2 μm, are produced. These powders were also characterized by SEM and the corresponding results are reported in supplementary Figure S1. The obtainment of few micrometers sized particles is confirmed. Moreover, EDS maps results agree with XRD analysis outcomes, with transition metals, particularly Ti, Nb and Mo, not homogeneously distributed in the powders, to indicate that the synthesis of the desired phases is not achieved by SHS. As observed in previous works focused on the fabrication of various additive free HEBs [17,18], the SHS process evolves too rapidly (few seconds) to allow for the complete diffusion of the five metallic constituents across the sample.

Table 2. Particle size characteristics, as determined by laser scattering analysis, of the SHS powders to be consolidated by SPS.

System ID	d_{10} (μm)	d_{50} (μm)	d_{90} (μm)	$d_{average}$ (μm)
HEB_Nb-SiC	0.155±0.025	0.825±0.215	6.645±1.055	2.185±0.395
HEB_Zr-SiC	0.13±0.01	0.61±0.04	5.715±0.435	1.88±0.15

Preprints (www.preprints.org) | NOT PEER-REVIEWED | Posted: 22 December 2023 doi:10.20944/preprints202312.1708.v1

Let's now consider the densification step. The sample shrinkage time profile recorded during SPS is compared in Figure 5 with data obtained when the SiC free HEB_Nb based powders, prepared according to Barbarossa et al. [18], were consolidated using the same operating parameters (T_D=1800 °C, HR=200°C/min, t_D=20 min, P=20 MPa). The markedly higher densification rate and the superior final sample shrinkage observed with the SiC containing powders confirmed the role played by the additive as sintering aid. It is also observed that, under such conditions, the consolidation of HEB_Nb-SiC is basically confined to the non-isothermal step, whereas only negligeable changes are manifested in sample shrinkage at the dwell temperature. In contrast, additive free powders continue their densification, albeit at a slower rate, also during the isothermal stage.

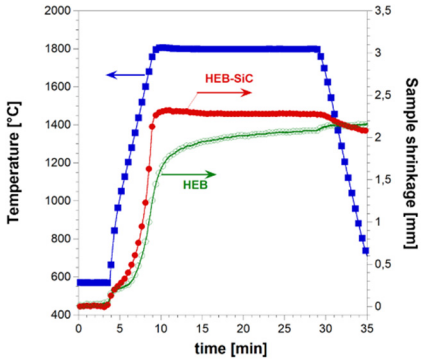

Figure 5. Comparison of sample shrinkage recorded during the preparation of dense HEB_Nb by SHS-SPS in presence or without SiC (T_D=1800 °C, HR=200°C/min, t_D=20 min, P=20 MPa). The corresponding temperature profile is also shown.

The benefit determined by the presence of SiC is also proved by the relative densities of the final products, i.e. 91.9±0.09% (HEB_Nb) and 98.7±0.7% (HEB_Nb-SiC), respectively.

The effect of the dwell temperature on product density is reported in Figure 6 for two holding time values (5 and 20 min). The extremely low densification level achieved at 1500°C/5min (72.3%) was progressively improved up to 98.3% as the sintering temperature was increased to 1900°C. Similar relative densities were also achieved at lower temperatures (1700°C), when the holding time was prolonged to 20 min. In the latter case, a further increase of T_D to 1800 and 1900°C did not determine additional beneficial effects, at least from the sample densification viewpoint.

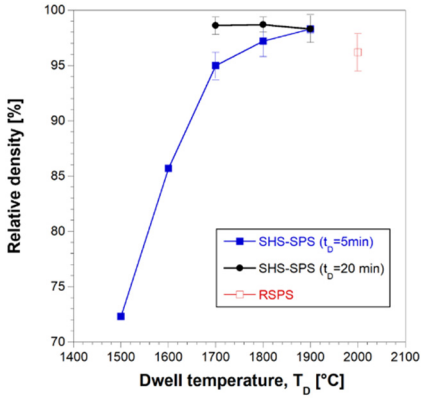

Figure 6. Effect of the dwell temperature on the relative density bulk HEB_Nb-SiC samples obtained by SHS-SPS when t_D=5 and 20 min (HR=200°C/min, P=20 MPa). Data obtained with the R-SPS approach are also reported.

The XRD patterns of bulk samples sintered at different T_D values are shown in supplementary Figures S2a and S2b for the cases of t_D equal to 5 and 20 min, respectively. Product composition is gradually improved as the holding temperature is progressively raised. The presence of secondary phases was detected in SPS products obtained when operating at 1700°C or lower dwell

Preprints (www.preprints.org) | NOT PEER-REVIEWED | Posted: 22 December 2023 doi:10.20944/preprints202312.1708.v1

temperatures. Samples prepared at 1800°C/20min, 1900°C/5min, and 1900°C/20min were more accurately analyzed by XRD using the Rietveld analytical procedure. The obtained results are reported in Figures 4b-4d and supplementary Table S3. The sample obtained at 1800°C/20 min is characterized by a single solid solution phase (83.1 wt.%), together with SiC (13.6 wt.%), mainly formed during the SHS reactions. Small amounts of HfO_2 and traces of C (2.4 and 0.9 wt.%, respectively) were also detected. Therefore, the secondary metal diborides found in the synthesized powders are all completely transformed into the expected HEB_Nb phase during SPS. Furthermore, the metal silicide phase ($MoSi_2$) also produced by SHS as a consequence of the chemical interaction of Si and Mo precursors (cf. reaction (1)) was not detected in the SPS product. The obtainment of the desired HEB_Nb-SiC composite is further verified in samples processed at 1900°C/5min and 1900°C/20min. The Rietveld analysis (Table S3) also evidenced that crystallite size of the produced HEB phase progressively increases as the sintering conditions become more severe, i.e. about 109 nm (1800/20min), 132 nm (1900/5min), and 152 nm (1900, 20 min).

SEM micrographs and corresponding elemental EDS maps shown in Figures 7 (t_D=5 min) and 8 (t_D=20 min) are consistent with XRD analysis results. Indeed, a T_D value of 1700°C was not sufficient to promote adequately diffusion phenomena in the sample undergoing SPS. Under such condition, an extension of the holding time from 5 min (Figure 7a) to 20 min (Figure 8a) did not produce appreciable improvements. On the other hand, as the temperature was raised to 1800°C (Figures 7b and 8b) and 1900°C (Figures 7c and 8c), significant gains in product microstructure were correspondingly achieved.

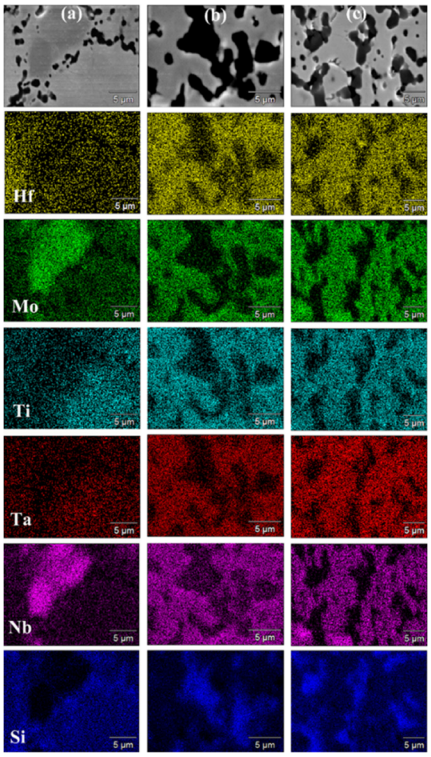

Figure 7. SEM micrographs and related elemental EDS maps of HEB_Nb-SiC samples obtained by SPS at t_D=5min for different T_D values (P=20MPa, HR=200°C/min) from SHS powders: (a) 1700°C, (b) 1800°C, and (a) 1900°C.

Preprints (www.preprints.org) | NOT PEER-REVIEWED | Posted: 22 December 2023 doi:10.20944/preprints202312.1708.v1

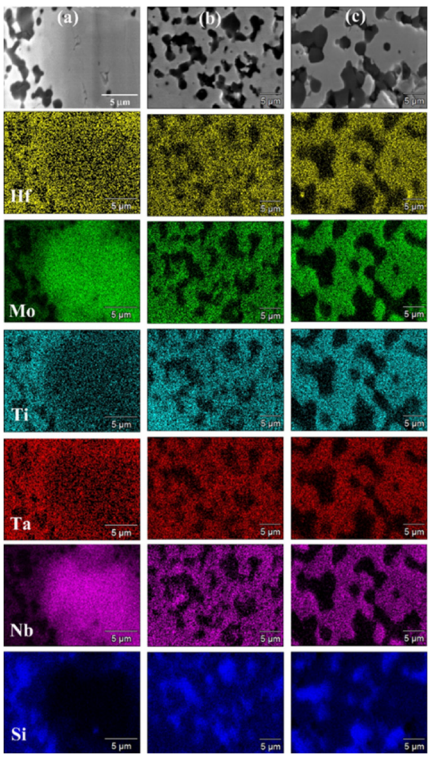

Figure 8. SEM micrographs and related elemental EDS maps of HEB_Nb-SiC samples obtained by SPS at t_D=20min for different T_D values (P=20MPa, HR=200°C/min) from SHS powders: (a) 1700°C, (b) 1800°C, and (a) 1900°C.

3.2.2. The $(Hf_{0.2}Mo_{0.2}Ti_{0.2}Ta_{0.2}Zr_{0.2})B_2$-SiC system

Based on the experimental findings attained with the HEB_Nb-SiC system, the preparation of bulk $(Hf_{0.2}Mo_{0.2}Ti_{0.2}Ta_{0.2}Zr_{0.2})B_2$-SiC was performed by SHS-SPS. Initial precursors (cf. Eq. (1) with Me=Zr) were reacted by SHS for the preparation of powders that were subsequently densified by SPS at 1800°C (20min/20 MPa), i.e. the optimal T_D value which allowed us to produce the desired Nb containing ceramic composite. The resulting sintered samples possessed a relative density equal to 97.7±0.6%. As for the composition, also in this case, the SHS reaction (1) did not go to completion, with the synthesized powders consisting of multiple phases. The latter ones were identified by XRD, and the corresponding content estimated by Rietveld analysis, whose results are reported in Figure 9a and supplementary Table S4. Other than the prescribed HEB (11.9 wt.% only) and SiC (10.9 wt.%) phases, the SHS product was rich of various individual and binary diborides (ZrB_2, TaB_2, HfB_2, MoB_2, TiB_2, $(MoTi)B_4$) along with other undesired species ($MoSi_2$, SiO_2, C, Si, B_4C).

However, as shown in Figure 9b, the complete conversion of the secondary phases into the desired ceramic composite was attained during SPS. Specifically, as evidenced by the Rietveld analysis (supplementary Table S4), the sintered sample basically consisted of $(Hf_{0.2}Mo_{0.2}Ti_{0.2}Ta_{0.2}Zr_{0.2})B_2$ (84.4 wt.%), and SiC (14.1 wt.%), with only a small amount of HfO_2 (1.5 wt.%). As for the case of the HEB_Nb system, it is also confirmed that no silicide phases were found in the sintered samples, being initial Si precursor finally converted into the corresponding carbide. SEM/EDS observations are in accordance with XRD analysis. In the latter regard, Figure 10 evidenced that all metallic elements are very homogeneously distributed into the HEB matrix, with the secondary phase uniformly dispersed across the sample volume. SEM micrographs also testify the high densification level achieved after SPS, with some surface porosity mostly due to grain pulling-out occurring during the polishing procedure. Also in this case, it should be noted that the sintering temperature required by Barbarossa et al. [17] to obtain approximately 97% dense additive free $(Hf_{0.2}Mo_{0.2}Ti_{0.2}Ta_{0.2}Zr_{0.2})B_2$ was significantly higher (1950°C) than that required in this work (1800°C)

Preprints (www.preprints.org) | NOT PEER-REVIEWED | Posted: 22 December 2023 doi:10.20944/preprints202312.1708.v1

for the preparation of the composite. Therefore, the role played by SiC as sintering aid is, once more, ascertained.

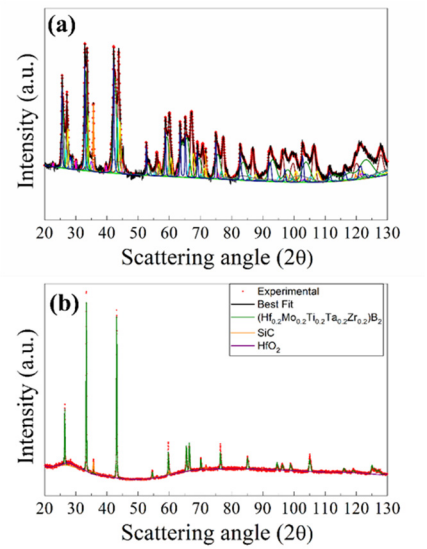

Figure 9. XRD patterns of HEB_Zr-SiC powders obtained by SHS (a) along with the corresponding SPS product (b) obtained at T_D=1800°C, HR=200°C/min, t_D=20min, P=20MPa.

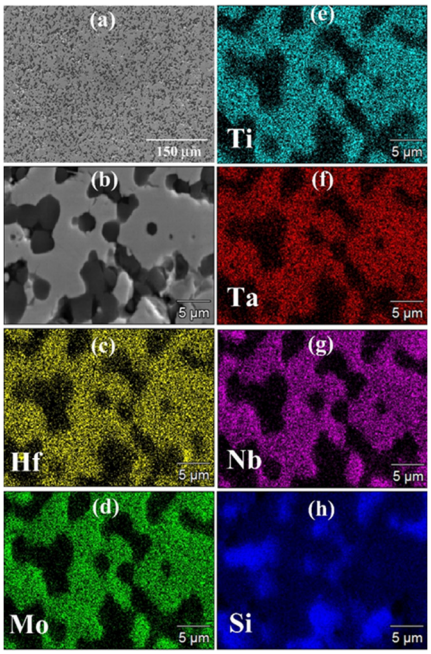

Figure 10. General (a) and detailed (b) SEM views along with the corresponding Hf (c), Mo (d), Ti (e), Ta (f), Nb (g), and Si (h) EDS maps of the HEB_Zr-SiC sample obtained by SPS (T_D =1800°C, t_D=20min, P=20MPa, HR=200°C/min) from powders synthesized by SHS according to reaction (1) with Me=Zr.

3.3. Oxidation behavior

The oxidation resistance of the two HEB-SiC ceramics obtained in this work was evaluated based on their behavior during 1h heat treatment in air furnace at different temperature conditions, in the range 600-1300°C. For the sake of comparison, the corresponding additive-free samples were also tested.

As shown in supplementary Figure S2, HEB_Nb and HEB_Zr specimens markedly change their appearance upon the oxidation test, with their original grey-brown color which turns first to grey blue (700°C) and then to orange (1200-1300°C). On the other hand, minor differences were observed in SiC-containing samples, which apparently seem to be less affected by the received heat treatment.

Preprints (www.preprints.org) | NOT PEER-REVIEWED | Posted: 22 December 2023 doi:10.20944/preprints202312.1708.v1

As observed in Figure 11, negligible weight changes were observed in all samples heat treated up to 700°C, regardless the presence of the additive. On the other hand, the latter play a key role when the samples were exposed to higher thermal levels. Indeed, pure HEBs lose progressively their weight as the temperature was increased to 1200°C and, above all, 1300°C. This feature can be ascribed to the volatilization of some oxidation products, as discussed later. In contrast, the presence of SiC apparently inhibits such volatilization phenomena, with the composite ceramics, particularly HEB_Zr-SiC, which display a gradual mass increase with temperature.

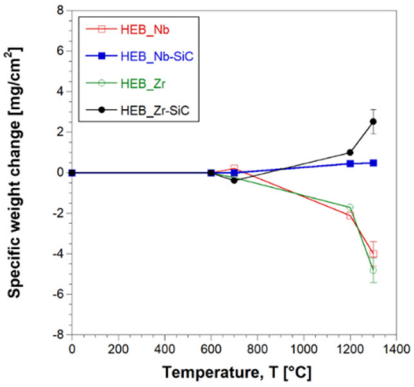

Figure 11. Weight change per surface area of HEB_Nb-SiC HEB_Zr-SiC samples obtained by SPS (T_D=1800°C, HR=200°C/min, t_D=20min, P=20MPa) during oxidation tests carried out at different temperatures in air furnace. Data relative to additive free HEB_Nb and HEB_Zr are also plotted, for the sake of comparison.

Compositional changes occurring on the surface of the samples annealed at various temperatures were evaluated by XRD analysis. The results obtained with HEB_Nb and HEB_Nb-SiC systems are shown in Figure 12. Up to 600°C, composition remained basically unaltered, except for the presence of very small peaks associated to MoO_3 and $TiTa_2O_7$, which indicates the incipient oxidation of the two ceramics. When temperature was raised to 700°C, the XRD patterns changed markedly, particularly for the SiC-free material. Under such condition, MoO_3 and $TiTa_2O_7$ peaks intensity increases, and two additional oxides (HfO_2, TiO_2) are detected by this analysis, to testify the oxidation progress. The same oxides were also found on the surface of the HEB_Nb-SiC specimen, but their intensity, particularly that of HfO_2, was much lower, while HEB is still the dominant phase. The latter finding provides a first evidence of the beneficial presence of SiC in the ceramic. The fact that minor weight changes are observed up to 700°C (Figure 11) indicate that, up to this stage, oxidation phenomena are confined to small sample volume. As specimens were heat treated at 1200°C, the two systems behave quite differently. As for HEB_Nb, the mixed oxide ascribed to $TiTa_2O_7$ was the only phase clearly detected by XRD. Almost an identical situation is also encountered at 1300°C. As also observed in previous works [7], some of the formed oxides, such as MoO_3, are volatile, so that they tend to disappear at such temperature levels. This feacture can be considered the reason for the corresponding weight decrease observed for this system (Figure 11). On the other hand, SiC introduction makes oxidation behavior of the ceramic particularly different at 1200-1300°C. Some silicate phases, either crystalline, such as $HfSiO_4$, detected by XRD analysis (Figure 12b) or amorphous, are formed. The latter phases are expected to incorporate various oxides, including the volatiles ones, so that they are not allowed to leave the sample. This fact can be readily correlated to the mass gained of HEB_Nb-SiC observed in Figure 11. A similar behavior was also observed with the Zr containing system. Therefore, the addition of SiC to HEB phases clearly impedes the progressive loss of volatile oxides formed when these ceramics are exposed to oxidation environments at high temperatures.

Preprints (www.preprints.org) | NOT PEER-REVIEWED | Posted: 22 December 2023 doi:10.20944/preprints202312.1708.v1

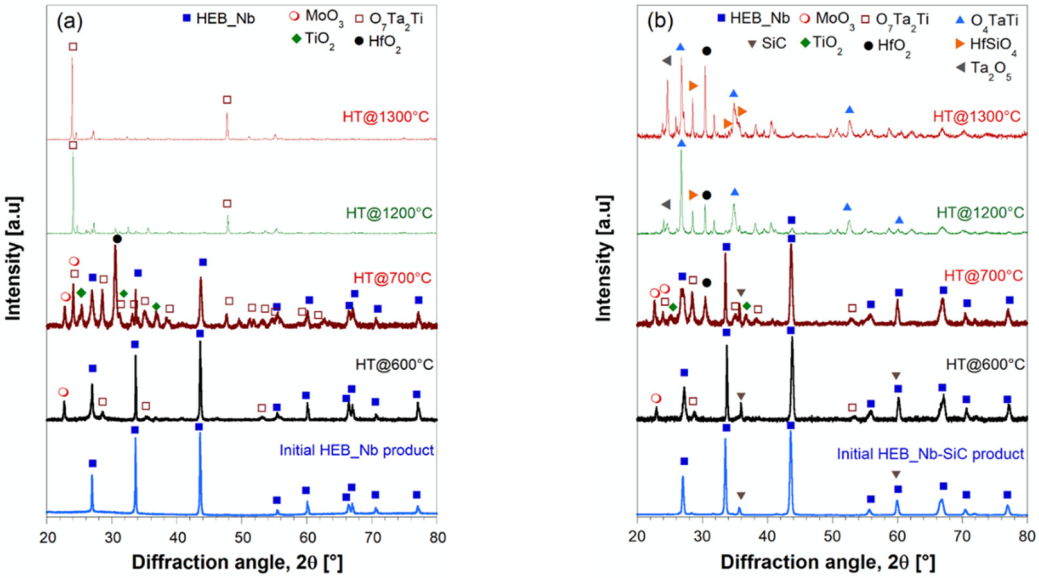

Figure 12. XRD patterns of HEB_Nb (a) and HEB_Nb-SiC (b) samples after being heat treated in air furnace at different temperatures. Apart from HEB and SiC, the other crystalline phases identified by XRD analysis in the oxidized samples and the related COD cards are: MoO_3 (1538963), O_7Ta_2Ti (4343510), O_4TaTi (2002580), HfO_2 (1545064), TiO_2 (9004144), Ta_2O_5 (2102123), and $HfSiO_4$ (9000852).

3.4. Mechanical properties

Table 3 reports Vickers hardness, and fracture toughness values measured for the different SiC-containing and additive-free HEB_Nb and HEB_Zr samples fabricated in this work under the diverse conditions necessary to produce the desired quinary diboride and SiC phases. The available literature data on different HEB-SiC bulk ceramics are also included in this table, along with the corresponding fabrication routes and processing conditions. It is apparent that the introduction of SiC to the HEB_Nb system provides a significant improvement in the K_{IC} value. As expected, the presence of the carbide phase leads to the deflection and branching of the cracks formed by Vickers indentation. Less is the distance between the SiC-phases distributed in the HEB-matrix higher is the fracture toughness of the system.

Table 3 also evidences that fracture toughness decreases as the sintering conditions becomes progressively more severe, i.e. 7.35 MPa $m^{1/2}$ (1800°C/20min), 6.23 MPa $m^{1/2}$ (1900°C/5min), and 5.36 MPa $m^{1/2}$ (1900°C/20min). This finding can be likely ascribed to the grain growth correspondingly taking place, as testified by the increased crystallite size of the HEB phase (cf. Table S3). As for the measured Vickers hardness, it remained roughly the same, in the range 26-27 GPa. A marked improvement in fracture toughness, albeit at a lower level with respect to the HEB_Nb-based system, was also found when adding SiC to the HEB_Zr matrix.

The effect of the introduction of 20 vol.% SiC on the HEB_Nb system was investigated by Zhang et al. [14]. A slightly higher HV value, compared to that obtained in this work, (28.1±0.9 instead of 27.0±1.7 GPa, respectively) was obtained in the latter study. This could be likely motivated by the more severe SPS conditions (T_D=2000°C) adopted to consolidate their BCR powders but also to the lower SiC content (20 instead of 27.7 vol.%) present in the ceramic. In contrast, the measured K_{IC} value was significantly higher in our study. This fact can be ascribed not only to the lower SiC fraction, but also to possible negative effects produced by grain growth taking place when the sample is exposed to high sintering temperatures. No further studies can be found in the literature on HEB_Nb-SiC and HEB_Zr-SiC composite formulations. When the comparison is extended to the other similar systems reported in Table 3, it can be stated that the composite ceramics produced in this work by SHS-SPS generally exhibits superior HV and K_{IC} properties. This outcome can be attributed to various causes, first the different nominal composition of the HEB phase and SiC content, the use of alternative synthesis methods for powders preparation (BR and BCR), as well as to the applied sintering

Preprints (www.preprints.org) | NOT PEER-REVIEWED | Posted: 22 December 2023 doi:10.20944/preprints202312.1708.v1

conditions. All these aspects are co-responsible for determining the performances of the produced material. For instance, the fact that, in the present work, the secondary SiC phase is directly synthesized *in-situ* (during SHS and SPS stages), instead of adding it after powder preparation by BR/BCR [12–14,16], is expected to be highly beneficial to establish stronger interfaces with the HEB matrix, and, in turn, improve mechanical properties of the ceramic. So far, the only literature study on HEB-SiC composites adopting a similar approach was focused on the direct synthesis by BR of the (V,Ti,Ta,Nb)B_2-SiC composite starting from V_2O_5, TiO_2, Ta_2O_5, Nb_2O_5, B_4C, carbon black, and Si [15]. Nonetheless, apart from the different route and HEB composition, compared to those considered in this work, the latter work was addressed only to the powder preparation. In any case, as clearly demonstrated in Licheri et al. [29], the co-synthesis of the different phases involved in a ceramic composite provides beneficial effects with respect to their combination as individual constituents.

Table 3. Particle size characteristics, as determined by laser scattering analysis, of the SHS powders to be consolidated by SPS.

System	Fabrication method	Sintering conditions (T_D, t_d, P)	ρ (%)	HV (GPa)	K_{IC} (MPa $m^{1/2}$)	Reference
$(Hf_{0.2}Mo_{0.2}Ti_{0.2}Ta_{0.2}Nb_{0.2})$-0 vol.%SiC	SHS-SPS	1950°C/2 min/20MPa	97.4±0.3	27.0±1.3	2.61±0.17	This work
$(Hf_{0.2}Mo_{0.2}Ti_{0.2}Ta_{0.2}Nb_{0.2})$-27.7 vol.%SiC	SHS-SPS	1800°C/20min/20MPa	97.2±1.4	26.0±1.0	7.35±0.66	This work
	SHS-SPS	1900°C/5 min/20MPa	98.3±1.3	27.0±1.7	6.23±0.50	This work
	SHS-SPS	1900°C/20min/20MPa	98.3±1.2	27.0±1.7	5.36±0.37	This work
$(Hf_{0.2}Mo_{0.2}Ti_{0.2}Ta_{0.2}Zr_{0.2})B_2$-0 vol.%SiC	SHS-SPS	1950°C/20min/20MPa	96.5±0.7	25.0±1.6	2.11±0.15	This work
$(Hf_{0.2}Mo_{0.2}Ti_{0.2}Ta_{0.2}Zr_{0.2})B_2$-27.4 vol.%SiC	SHS-SPS	1800°C/20min/20MPa	97.7±0.6	27.0±1.5	4.11±0.32	This work
$(Hf_{0.2}Mo_{0.2}Ti_{0.2}Ta_{0.2}Nb_{0.2})$-20 vol.%SiC	BR-SPS	2000°C/10min/30MPa	99.1±0.1	26.2±1.8	4.41±0.21	[14]
	BCR-SPS		100.0±0.5	28.1±0.9	4.25±0.37	
$(Hf_{0.2}Mo_{0.2}Ti_{0.2}Zr_{0.2}Nb_{0.2})$-20 vol.%SiC	BR-SPS	2000°C/10min/30MPa	100.0±0.4	25.8±1.2	4.53±0.66	[14]
	BCR-SPS		98.6±0.2	29.0±1.3	3.80±0.33	
$(Hf_{0.2}Nb_{0.2}Ti_{0.2}Ta_{0.2}Zr_{0.2})B_2$-10 vol.%SiC	BCR-SPS	1800°C/10min/30MPa	99.47	~ 20.1	~ 5.00	[16]
$(Hf_{0.2}Nb_{0.2}Ti_{0.2}Ta_{0.2}Zr_{0.2})B_2$-20 vol.%SiC	BCR-SPS	1800°C/10min/30MPa	99.51	~ 20.7	~5.20	[16]
	BCR-HP	1800°C/60 min/n.r.	> 99	22.8±1.2	4.85±0.33	[13]
	BCR-SPS	1600-1900°C/10min/30MPa	> 97	~23	~4.7	[12]
$(Hf_{0.2}Nb_{0.2}Ti_{0.2}Ta_{0.2}Zr_{0.2})B_2$-30 vol.%SiC	BCR-SPS	1800°C/10min/30MPa	99.73	~ 21.1	~5.20	[16]

4. Conclusions

Dense $(Hf_{0.2}Mo_{0.2}Ti_{0.2}Ta_{0.2}Nb_{0.2})B_2$-SiC and $(Hf_{0.2}Mo_{0.2}Ti_{0.2}Ta_{0.2}Zr_{0.2})B_2$-SiC were synthesized in this work starting from elemental transition metals, B_4C and Si. While powder synthesis and consolidation in one processing step by reactive SPS (2000°C/20min/20MPa) did not succeed in achieving the prescribed HEB and SiC phases, this goal was reached with the SHS-SPS route. Although initial precursors were only partially converted by SHS, the completion of the synthesis reaction was attained by SPS under the optimized condition of 1800°C/20min/20MPa. Sintered samples of both HEB-SiC systems possessed relative densities higher than 97% and did not contain secondary borides. Only small amounts of oxides (1.1-2.4 wt.%) were detected. The introduction of SiC was found to be highly beneficial to improve sintering behavior, mechanical, and oxidation resistance properties, compared to the corresponding additive free high-entropy borides. In particular, superior fracture toughness was displayed by the Nb-containing system processed by SPS at 1800°C/20min, whereas an increase of the sintering temperature determined a gradual decrease in

this property. Very important, the presence of SiC was found to protect the material during samples heat-treatment in air, playing a prominent role in hindering the volatilization of the produced metal oxides like MoO_3, so that the corresponding material weight loss can be avoided or retained. Other than the intrinsic benefits induced by the use of this additive, a positive effect derives by the *in-situ* synthesis of both ceramic constituents during the SHS and SPS stages. This is expected to highly promote the establishment of strong interfaces between the formed phases and, consequently, enhance the performances of resulting material.

Supplementary Materials: The following supporting information can be downloaded at the website of this paper posted on Preprints.org, Figure S1: (a) SEM micrograph along with the corresponding EDS elemental maps, and (b) X-EDS pattern of HEB_Nb-SiC powders synthesized by SHS; Figure S2: XRD patterns of HEB_Nb-SiC products obtained by SHS-SPS at different T_D values: (a) t_D=5 min, (b) t_D=20 min. The XRD pattern of SHS powders is also included, for comparison; Figure S3: Optical images (complete and detailed view) showing the surface changes of $(Hf_{0.2}Mo_{0.2}Ti_{0.2}Ta_{0.2}Nb_{0.2})B_2$ and $(Hf_{0.2}Mo_{0.2}Ti_{0.2}Ta_{0.2}Nb_{0.2})B_2$-SiC samples after oxidation experiments in air furnace at different temperatures; Figure S4: Optical images (complete and detailed view) showing the surface changes of $(Hf_{0.2}Mo_{0.2}Ti_{0.2}Ta_{0.2}Zr_{0.2})B_2$ and $(Hf_{0.2}Mo_{0.2}Ti_{0.2}Ta_{0.2}Zr_{0.2})B_2$-SiC samples after oxidation experiments in air furnace at different temperatures; Table S1: Phases and quantitative phase analysis results of the HEB_Nb-SiC product obtained by Reactive SPS. (SS): Solid Solution; Table S2: Phases and quantitative phase analysis results of the HEB_Nb-SiC product obtained by SHS; Table S3: Phases and quantitative phase analysis results of the HEB_Nb-SiC products obtained by SPS, at different operating conditions, from SHS powders; Table S4: Phases and quantitative phase analysis results of the HEB_Zr-SiC products obtained by SHS, and SPS.

Author Contributions: Conceptualization, R.O. and R.L.; methodology, R.O., R.L., S.G., and E.P.; investigation, E.P., R.L., S.G., P.F.; resources, G.C. and R.O.; writing—original draft preparation, R.O.; writing—review and editing, R.O., R.L., S.G., E.P., P.F.; supervision, R.O., R.L., G.C.; funding acquisition, G.C., and R.O. All authors have read and agreed to the published version of the manuscript."

Funding: This research was funded by Italian Ministry for Research and Education (MUR) under the National Recovery and Resilience Plan (PNRR) – MISSION 4 COMPONENT 2, "From research to business" INVESTMENT 1.5, "Creation and strengthening of Ecosystems of innovation" and construction of "Territorial R&D Leaders", project eINS- Ecosystem of Innovation for Next Generation Sardinia (cod. ECS 00000038) and by the Italian Ministry for Research and Education (MUR), project I-CREATE - Innovative Class of REfrActory ceramics for extreme Environments" (PRIN-2022, CUP. F53D23002020006.

Data Availability Statement: Data are contained within the article and supplementary materials.

Acknowledgments: The authors are grateful to Giacomo Mazzacavallo from University of Padova, Italy, for his support in mechanical test performing. The contribution of Dr. Simone Barbarossa from University of Palermo, Italy, is also gratefully acknowledged.

Conflicts of Interest: The authors declare no conflict of interest.

References

1. Fahrenholtz, W.G.; Wuchina, E.J.; Lee, W.E.; Zhou, Y. Ultra-High Temperature Ceramics: Materials for Extreme Environment Applications, 1st ed.; Wiley-American Ceramic Society, Hoboken, New Jersey, U.S., 2014; pp. 1–441.
2. Fahrenholtz, W.G.; Hilmas, G.E.; Talmy, I.G.; Zaykoski, J.A. Refractory diborides of zirconium and hafnium *J. Am. Ceram. Soc.* **2007**, *90 (5)*, pp. 1347-1364.
3. Licheri, R.; Orrù, R.; Musa, C.; Cao, G. Efficient technologies for the fabrication of dense TaB_2-based ultra-high-temperature ceramics. *ACS Applied Materials and Interfaces* **2010**, *2(8)*, 2206-2212.
4. Sciti, D.; Balbo, A.; Bellosi, A. Oxidation behaviour of a pressureless sintered HfB2-MoSi2 composite. *Journal of the European Ceramic Society* **2009**, *29(9)*, 1809–1815.
5. Musa, C.; Licheri, R.; Orrù, R.; Cao, G. Synthesis, sintering, and oxidative behavior of HfB_2-$HfSi_2$ ceramics. *Industrial and Engineering Chemistry Research* **2014**, *53(22)*, 9101-9108.
6. Aguirre, T.G.; Lamm, B.W.; Cramer, C.L.; Mitchell, D.J. Zirconium-diboride silicon-carbide composites: A review. *Ceramics International* **2022**, *48(6)*, 7344–7361.
7. Gild, J.; Zhang, Y.; Harrington, T.; Jiang, S.; Hu, T.; Quinn, M.C.; Mellor, W.M.; Zhou, N.; Vecchio, K.; Luo, J. High-Entropy Metal Diborides: A New Class of High-Entropy Materials and a New Type of Ultrahigh Temperature Ceramics. *Sci. Rep.* **2016**, *6*, 37946.

8. Mayrhofer, P.H.; Kirnbauer, A.; Ertelthaler, P.; Koller, C.M. High-entropy ceramic thin films; A case study on transition metal diborides. *Scripta Mater.* **2018,** *149*, 93-97.
9. Tallarita, G.; Licheri, R.; Garroni, S.; Barbarossa, S.; Orrù, R.; Cao, G. High-entropy transition metal diborides by reactive and non-reactive spark plasma sintering: A comparative investigation. *J Eur Ceram Soc.* **2020**, *40*, 942-952.
10. Feng, L.; Fahrenholtz, W.G.; Brenner, D.W. High-Entropy Ultra-High-Temperature Borides and Carbides: A New Class of Materials for Extreme Environments. *Annual Review of Materials Research* **2021**, *51*, 165-185.
11. Wang, F.; Monteverde, F.; Cui, B. Will high-entropy carbides and borides be enabling materials for extreme environments? *International Journal of Extreme Manufacturing* **2023**, *5(2)*, 022002.
12. Shen, X.Q.; Liu, J.X., Li, F.; Zhang, G.J. Preparation and characterization of diboride-based high entropy $(Ti_{0.2}Zr_{0.2}Hf_{0.2}Nb_{0.2}Ta_{0.2})B_2$–SiC particulate composites. *Ceram. Int*. **2019**, *45(18)*, 24508-24514.
13. Liu, J.X.; Shen, X.Q.; Wu, Y., Li, F., Liang, Y., Zhang, G.J. Mechanical properties of hot-pressed high-entropy diboride-based ceramics. *J. Adv. Ceram.* **2020**, *9(4)*, 503–510.
14. Zhang, Y.; Sun, S.K.; Guo, W.M.; Xu, L.; Zhang, W.; Lin, H.T. Optimal preparation of high-entropy boride-silicon carbide ceramics. *J. Adv. Ceram.* **2021**, *10(1)*, 173–180.
15. Gong, Y.; Yang, Z.; Wei, X.; Song, S.; Ma, S. Synthesis and electromagnetic wave absorbing properties of high-entropy metal diboride-silicon carbide composite powders. *J. Mater. Sci.* **2022**, *57(20)*, 9218–9230.
16. Cheng, Y.Y.; Zhou, L.; Liu, J.X.; Tan, Y.F.; Zhang, G.J. Grain growth inhibition by sluggish diffusion and Zener pinning in high-entropy diboride ceramics. *J. Am. Ceram. Soc.* **2023**, *106(8)*, 4997–5004.
17. Barbarossa, S.; Orrù, R.; Garroni, S.; Licheri, R.; Cao, G. Ultra High Temperature High-Entropy Borides: Effect of Graphite Addition on Oxides Removal and Densification Behaviour. *Ceram. Int.* **2021**, *47(5)*, 6220-6231.
18. Barbarossa, S.; Orrù, R.; Cannillo, V.; Iacomini, A.; Garroni, S.; Murgia, M.; Cao, G. Fabrication and Characterization of Quinary High Entropy-Ultra-High Temperature Diborides. *Ceramics* **2021**, 4, 108–120.
19. Cincotti, A., Licheri, R.; Locci, A.M.; Orrù, R.; Cao, G. A review on combustion synthesis of novel materials: recent experimental and modeling results. *J. Chem. Technol. Biotechnol.* **2003**, *78*, 122-127.
20. Matthews, F.L.; Rawlings R. Composite Materials: Engineering and Science, 1st ed.; Woodhead Publishing: Sawston, Great Britain, 1999; pp. 1-480.
21. Shackelford, J.F.; Alexander, W. CRC Materials Science and Engineering Handbook, 3rd ed.; CRC press: Boca Raton, Florida, U.S., 2001; pp. 1-1980.
22. Lutterotti, L.; Ceccato, R.; Dal Maschio, R.; Pagani, E. Quantitative analysis of silicate glass in ceramic materials by the Rietveld method. *Mater. Sci. Forum* **1998**, *87*, 278-281.
23. Ponton, C.B.; Rawlings, R.D. Vickers Indentation Fracture Toughness Test. Part 1: Review of Literature and Formulation of Standardised Indentation Toughness Equations. *Mater. Sci. Technol.* **1989**, *5*, 865–872.
24. Ponton, C.B.; Rawlings, R.D. Vickers Indentation Fracture Toughness Test. Part 2: Application and Critical Evaluation of Standardised Indentation Toughness Equations. *Mater. Sci. Technol.* **1989**, *5*, 961–976.
25. Licheri, R.; Orrù, R.; Locci, A.M.; Cao, G. Efficient synthesis/sintering routes to obtain fully dense ultra-high-temperature ceramics (UHTCs). *Industrial and Engineering Chemistry Research* **2007**, *46(26)*, 9087-9096.
26. Orrù, R.; Cao, G. Comparison of reactive and non-reactive spark plasma sintering routes for the fabrication of monolithic and composite Ultra High Temperature Ceramics (UHTC) materials. *Materials* **2013**. *6(5)*, 1566-1583.
27. Licheri, R.; Musa, C.; Orrù, R.; Cao, G. Influence of the heating rate on the in situ synthesis and consolidation of ZrB_2 by reactive Spark Plasma Sintering. *Journal of the European Ceramic Society* **2015**, *35(4)*, 1129-1137.
28. Licheri, R.; Orrù, R.; Musa, C.; Locci, A.M.; Cao, G. Consolidation via spark plasma sintering of HfB_2/SiC and HfB_2/HfC/SiC composite powders obtained by self-propagating high-temperature synthesis. *Journal of Alloys and Compounds* **2009**, *478(1-2)*, 572-578.
29. Licheri, R.; Orrù, R.; Musa, C.; Cao, G. Combination of SHS and SPS Techniques for fabrication of fully dense ZrB2-ZrC-SiC composites. *Materials Letters* **2008**, *62(3)*, 432-435.